

A novel baseline perspective visibility graph for time series analysis

Huang-Jing Ni(倪黄晶), Zi-Jie Song(宋紫婕), Jiao-Long Qin(秦姣龙), Ye Wu(吴烨), Shi-Le Qi(戚世乐), and Ming Song(宋明)

Citation: Chin. Phys. B, 2025, 34 (**8**): 080504. DOI: 10.1088/1674-1056/adce9a
http://cpb.iphy.ac.cn; http://iopscience.iop.org/cpb

What follows is a list of articles you may be interested in

Transition to chaos in lid-driven square cavity flow

Tao Wang(王涛) and Tiegang Liu(刘铁钢)
Chin. Phys. B, 2021, 30 (**12**): 120508. DOI: 10.1088/1674-1056/ac3226

Patterns of cross-correlation in time series: A case study of gait trails

Jia Song(宋佳), Tong-Feng Weng(翁同峰), Chang-Gui Gu(顾长贵), Hui-Jie Yang(杨会杰)
Chin. Phys. B, 2020, 29 (**8**): 080501. DOI: 10.1088/1674-1056/ab9287

Extracting hidden weak sinusoidal signal with short duration from noisy data:Analytical theory and computational realization

Ying Zhang(张英), Zhaoyang Zhang(张朝阳), Hong Qian(钱弘), Gang Hu(胡岗)
Chin. Phys. B, 2017, 26 (**10**): 100508. DOI: 10.1088/1674-1056/26/10/100508

Multifractal modeling of the production of concentrated sugar syrup crystal

Sheng Bi(闭胜), Jianbo Gao(高剑波)
Chin. Phys. B, 2016, 25 (**7**): 070502. DOI: 10.1088/1674-1056/25/7/070502

Experimental identification of a comb-shaped chaotic region in multiple parameter spaces simulated by the Hindmarsh–Rose neuron model

Jia Bing (贾冰)
Chin. Phys. B, 2014, 23 (**3**): 030505. DOI: 10.1088/1674-1056/23/3/030505

A novel baseline perspective visibility graph for time series analysis

Huang-Jing Ni(倪黄晶)[1,2], Zi-Jie Song(宋紫婕)[3], Jiao-Long Qin(秦姣龙)[4], Ye Wu(吴烨)[4], Shi-Le Qi(戚世乐)[2,†], and Ming Song(宋明)[5,6,‡]

[1] *School of Computer Science, Nanjing University of Posts and Telecommunications, Nanjing* 210003, *China*
[2] *Key Laboratory of Brain-Machine Intelligence Technology, Ministry of Education, Nanjing University of Aeronautics and Astronautics, Nanjing* 211106, *China*
[3] *School of Chemistry and Life Sciences, Nanjing University of Posts and Telecommunications, Nanjing* 210003, *China*
[4] *Key Laboratory of Intelligent Perception and Systems for High-Dimensional Information of Ministry of Education, School of Computer Science and Engineering, Nanjing University of Science and Technology, Nanjing* 210094, *China*
[5] *Brainnetome Center, Institute of Automation, Chinese Academy of Sciences, Beijing* 100190, *China*
[6] *National Laboratory of Pattern Recognition, Institute of Automation, Chinese Academy of Sciences, Beijing* 100190, *China*

(Received 16 February 2025; revised manuscript received 7 April 2025; accepted manuscript online 21 April 2025)

The natural visibility graph method has been widely used in physiological signal analysis, but it fails to accurately handle signals with data points below the baseline. Such signals are common across various physiological measurements, including electroencephalograph (EEG) and functional magnetic resonance imaging (fMRI), and are crucial for insights into physiological phenomena. This study introduces a novel method, the baseline perspective visibility graph (BPVG), which can analyze time series by accurately capturing connectivity across data points both above and below the baseline. We present the BPVG construction process and validate its performance using simulated signals. Results demonstrate that BPVG accurately translates periodic, random, and fractal signals into regular, random, and scale-free networks respectively, exhibiting diverse degree distribution traits. Furthermore, we apply BPVG to classify Alzheimer's disease (AD) patients from healthy controls using EEG data and identify non-demented adults at varying dementia risk using resting-state fMRI (rs-fMRI) data. Utilizing degree distribution entropy derived from BPVG networks, our results exceed the best accuracy benchmark (77.01%) in EEG analysis, especially at channels F4 (78.46%) and O1 (81.54%). Additionally, our rs-fMRI analysis achieves a statistically significant classification accuracy of 76.74%. These findings highlight the effectiveness of BPVG in distinguishing various time series types and its practical utility in EEG and rs-fMRI analysis for early AD detection and dementia risk assessment. In conclusion, BPVG's validation across both simulated and real data confirms its capability to capture comprehensive information from time series, irrespective of baseline constraints, providing a novel method for studying neural physiological signals.

Keywords: baseline perspective visibility graph, degree distribution entropy, time series analysis
PACS: 05.45.Tp, 87.19.lf, 87.19.le, 05.10.–a
DOI: 10.1088/1674-1056/adce9a **CSTR:** 32038.14.CPB.adce9a

1. Introduction

The natural visibility graph (NVG) method is a technique that constructs a network based on the convexity of each data point in a time series.[1] This method can serve as a valuable link between signal processing and graph theory, allowing for the direct transformation of a time series into a complex network. To date, the NVG method has been widely used in physiological signal analysis, such as heartbeat,[2,3] electroencephalograph (EEG),[4,5] and functional magnetic resonance imaging (fMRI),[6] due to its straightforward calculation process, efficient time consumption, and ability to preserve the dynamic characteristics inherent in the time series.

In the NVG method, a one-to-one correspondence is established between each data point in a discrete time series and a node within the mapped graph, while the connectivity between data points is determined by a straightforward visibility criterion.[1] The mathematical formula for this visibility criterion in the NVG method can be expressed as follows: an edge connecting any two data points (t_a, y_a) and (t_b, y_b) in the time series can be established if all intermediate data points (t_c, y_c) satisfy $y_c < y_b + (y_a - y_b)[(t_b - t_c)/(t_b - t_a)]$, $\forall t_c : t_a < t_c < t_b$. This visibility criterion serves as the fundamental principle of the NVG method, enabling it to transform a time series into a complex network. However, the NVG algorithm can only be applied when all data points in the time series exhibit positive values (*i.e.*, above the baseline). If any data point falls below the zero baseline, direct utilization of the NVG formula would compromise the inherent structural characteristics of the original time series and deviate from the visibility criterion.[7] This limitation is illustrated in Fig. 1(b), where the connections between nodes above and below the baseline, as well as those between nodes below the baseline, are lost, while erroneous connections between nodes above and below

†Corresponding author. E-mail: shile.qi@nuaa.edu.cn
‡Corresponding author. E-mail: msong@nlpr.ia.ac.cn

© 2025 Chinese Physical Society and IOP Publishing Ltd. All rights, including for text and data mining, AI training, and similar technologies, are reserved.

the baseline are established. Specifically, according to the definition of the natural visibility graph in Ref. [1], there should be connections between the nodes positioned above and below the baseline in Fig. 1(b), such as A–F, C–E, C–H, D–F, and G–J. Besides, connections are also expected to exist among the nodes located below the baseline, such as C–F, C–G, C–I, F–I, and G–I. Nonetheless, these referred connections are lost in the conversion of NVG. Furthermore, incorrect connections are established between nodes above and below the baseline that should remain disconnected, such as A–C, B–D, and E–G. Consequently, the natural visibility graph algorithm fails to adequately capture connections of data points below the baseline, resulting in potential loss of crucial information within the time series.

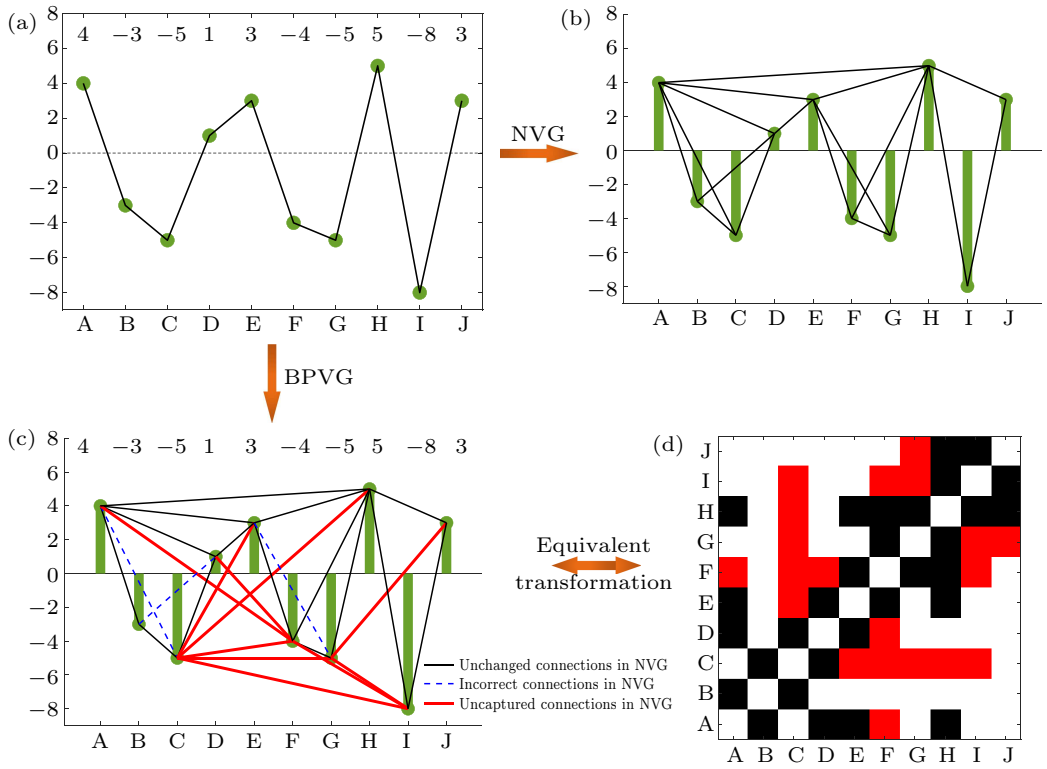


Fig. 1. The line chart for this simulation series. The transverse axis displays the assigned letter for each data point. (b) The corresponding NVG outcome. The black lines connecting the data points represent their connections, which are determined by directly applying the NVG algorithm. (c) The corresponding BPVG outcome. The actual connections determined by BPVG are represented by solid black and red lines. Red lines (*i.e.*, A–F, C–E, C–F, C–G, C–H, C–I, D–F, F–I, G–I, G–J) indicate uncaptured connections in the NVG outcome, while black lines remain consistent with those obtained by NVG. Blue dashed lines (*i.e.*, A–C, B–D, E–G) represent incorrect connections established in the NVG outcome that remain disconnected according to BPVG. (d) The corresponding adjacency matrix of the BPVG outcome is shown, with blocks colored in black and red corresponding to the same colors as the solid lines in subfigure (c).

Previous studies have demonstrated that signals below the baseline also contain crucial physiological information.[8–10] For instance, fMRI indirectly reflects neuronal activity by measuring the blood oxygen level dependent (BOLD) signal, while a negative BOLD signal may indicate changes in neuronal activity.[8] When analyzing event-related potentials, it might require to measure the amplitude distance between the negative peak of the component and the preceding positive peak to determine the magnitude of negative deflection independent of the baseline.[10,11] Therefore, signals below the baseline can reflect significant physiological information and constitute essential factors in physiological signal analysis.

In order to effectively utilize signals below the baseline in the visibility graph, a few researchers have made valuable explorations. Zheng *et al.*[7] introduced a weighted dual-perspective visibility graph, incorporating the calculation of NVGs for both the original and inverted time series, as well as their combination. Similarly, the study conducted by Hasson *et al.*[12] explored a combinatorial framework to quantify the asymmetries between the minimum and maximum values in local fluctuations of time series. This framework also involved constructing visibility graphs on both the original and flipped time series, respectively. The aforementioned two methods, however, only capture a fraction of the time series nodes exhibiting high absolute values, while neglecting the remaining time points below the baseline.

In this study, we commence with the definition of visibility graph, and propose a novel algorithm called the baseline perspective visibility graph (BPVG). The BPVG algorithm is designed to capture network connectivity information above and below the baseline at all time points, thus providing a more comprehensive analysis. To investigate the effectiveness of the BPVG algorithm, we conduct an analysis of simulation signals, examining the distinctive characteristics of networks

constructed using BPVG across various types of classical time series. Moreover, we extend our investigation to real EEG and resting state fMRI (rs-fMRI) time series, which may provide insights into complex dynamic characteristics.

2. Methods and materials

2.1. BPVG algorithm

The BPVG algorithm improves the definition of the connection in the NVG, thereby facilitating the handling of potential negative values in time series. An illustration of the construction of BPVG is provided in Fig. 1. Specifically, the process involves assigning each data point in the time series to individual nodes in the visibility graph, and then the criteria for establishing connections between these nodes are outlined as follows. Given any two data points (t_a, y_a) and (t_b, y_b) in a time series, for any intermediate data point (t_c, y_c), we have the relationship of $t_a < t_c < t_b$, and let $Y = y_b + (y_a - y_b)\frac{t_b - t_c}{t_b - t_a}$. Accordingly, the connection L_{ab} between the points (t_a, y_a) and (t_b, y_b) can be obtained by

$$L_{ab} = \begin{cases} 1, & (Y < 0 || Y > y_c, \ \forall y_c \geq 0) \ \text{ or} \\ & (Y > 0 || Y < y_c, \ \forall y_c < 0), \\ 0, & \text{otherwise.} \end{cases} \tag{1}$$

Thus, the BPVG outcome can be constructed for a given time series in this manner.

2.2. Entropy of degree distribution

In order to quantitatively characterize the degree distribution properties of the BPVG network, we employ the degree distribution entropy (E_{DD}) as a network feature. The degree of each node in BPVG corresponds to its number of connections. Consequently, E_{DD} can be calculated using $E_{DD} = -\sum_{k=0}^{k_{max}} p(k) \times \log p(k)$, where $p(k)$ represents the probability of the nodes having a degree k in BPVG, and k_{max} denotes the maximum value of k.

2.3. Generation of simulation time series

To investigate the characteristics of BPVG in classical time series, we conduct simulations on classical periodic, random, and fractal series. As suggested in Ref. [13], a sinusoidal signal is selected as a representative periodic series. Moreover, a typical random series can be generated by following a standard normal distribution $N(0,1)$. Additionally, the equation of fractional Brownian motion,

$$P\left\{\frac{f(x+\Delta x) - f(x)}{\|\Delta x\|^H} < t\right\} = F(t),$$

can generate fractal series with multiple fractal scales. In this equation, x represents a point in an E-dimensional Euclidean space, $F(t)$ denotes the distribution function of the random variable t which follows a standard normal distribution $N(0,1)$, $\|\Delta x\|$ represents the sampling interval, and H signifies the Hurst exponent.

2.4. Real EEG and rs-fMRI data

2.4.1. EEG data description and preprocessing

Furthermore, we employ BPVG on real EEG signals to evaluate its potential in distinguishing patients with Alzheimer's disease (AD) from healthy controls (HC). To this end, the publicly available database (OpenNeuro Dataset ds004504)[14,15] is analyzed, which contains resting-state EEG recordings from 29 HCs (67.9±5.4 years old; 18 male/11 female) and 36 patients with AD (66.4±7.9 years old; 12 male/24 female). The EEG signals were acquired using a Nihon Kohden EEG 2100 clinical device, with the sampling rate set at 500 Hz. According to the manual of the device, 19 scalp electrodes (*i.e.*, Fp1, Fp2, F7, F3, Fz, F4, F8, T3, C3, Cz, C4, T4, T5, P3, Pz, P4, T6, O1, and O2) based on the 10-20 international system were used, as well as two reference electrodes (*i.e.*, A1 and A2) were placed on the mastoids for impedance check. The recording duration for the HC group ranged from 12.5 min to 16.5 min, whereas the AD group exhibited a range of 5.1 min to 21.3 min. In order to ensure uniformity, only the initial 5-minute recordings were utilized for each subject in this study. Please refer to Ref. [16] for more detailed descriptions.

The preprocessed EEG signals released in the derivatives folder[17] were directly utilized in this study. In brief, the preprocessing pipeline consisted of the following steps: (i) applying a Butterworth band-pass filter with a range of 0.5 Hz–45 Hz and re-referencing the signals to A1–A2; (ii) removing data segments that exceeded the maximum acceptable standard deviation of 17 within a window of 0.5 seconds using the Artifact Subspace Reconstruction method; (iii) transforming the 19 EEG signals into 19 independent component analysis (ICA) components using the RunICA algorithm; (iv) excluding ICA components identified as "eye artifacts" or "jaw artifacts" through automatic classification using the ICLabel routine in the EEGLAB platform.

2.4.2. Rs-fMRI data description and preprocessing

Moreover, we also employ BPVG to explore its efficacy in identifying non-demented adults with varying dementia risk using real rs-fMRI data. The publicly available dataset (OpenNeuro Dataset ds004796)[18] is subsequently analyzed. Initially, subjects with complete rs-fMRI, MRI, and genetic information on APOE and PICALM variants were selected. Participants without APOE-ε4/PICALM GG alleles were categorized into the no-risk group, whereas those carrying APOE-ε4 and PICALM *GG* alleles were classified as the double-risk group. This study included 27 subjects in the no-risk group (mean age 55.2±2.9 years, 15 male/12 female) and 16 subjects in the double-risk group (mean age 55.3±3.0 years, 6 male/10 female). Closed-eye condition rs-fMRI scans were performed for each subject using a 3T Siemens scanner. The rs-fMRI scanning parameters were: acquisition of 560 time points with a repetition time (TR) of 0.8 s, an echo time

(TE) of 0.038 s, a flip angle (FA) of 52°, and a voxel size of 2 mm×2 mm×2 mm. The MRI scans were conducted with a TR of 2.4 s, TE of 2.74 ms, FA of 8°, and a voxel size of 0.8 mm×0.8 mm×0.8 mm. A more detailed descriptions can be found in Ref. [18].

The Data Processing Assistant for Resting-State fMRI Advanced (DPARSFA) toolbox[19,20] was employed to preprocess the functional imaging data. The initial ten volumes were discarded, and the remaining 550 volumes were corrected for slice timing and motion effects. Participants were not excluded if their motion did not exceed 3 mm of translation or 3° of rotation in any direction. The functional brain images were then normalized to the Montreal Neurological Institute (MNI) space using the Diffeomorphic Anatomical Registration Through Exponentiated Lie algebra (DARTEL) strategy[21] and resampled to a voxel size of 2 mm×2 mm×2 mm. Subsequently, nuisance covariates, including linear and quadratic trends, Friston 24 motion parameters, white matter signal, and cerebrospinal fluid signal, were regressed out. Finally, temporal filtering within the frequency range of 0.01 Hz–0.1 Hz was applied, followed by spatial smoothing with an isotropic Gaussian kernel of 4 mm.

2.5. BPVG analysis on EEG and rs-fMRI time series

2.5.1. BPVG analysis on EEG time series

As suggested in Ref. [16], the brain activity recorded from each channel was decomposed into five frequency bands of interest: Delta (0.5 Hz–4 Hz), Theta (4 Hz–8 Hz), Alpha (8 Hz–13 Hz), Beta (13 Hz–25 Hz), and Gamma (25 Hz–45 Hz). Subsequently, to effectively capture the dynamic characteristics of the EEG signals and optimize computational efficiency, each recording from every frequency band was segmented into non-overlapping time windows of 10 seconds duration. Consequently, BPVG analysis can thus be conducted on each segment within every frequency band for each channel, facilitating the calculation of E_{DD} features based on these BPVGs.

2.5.2. BPVG analysis on rs-fMRI time series

In order to perform BPVG analysis at the regions of interests (ROI) level, we adopted the Brainnetome atlas,[22] which covers 274 ROIs: 210 cortical, 36 subcortical, and 28 cerebellar. From these predefined ROIs, we extracted the regional mean time series for each ROI, and conducted BPVG analysis on these 274 time series for each subject.

2.5.3. Classification by using the E_{DD} feature

The E_{DD} features extracted from each segment within every frequency band for each EEG channel were concatenated and transformed into a vector. Subsequently, these resulting vectors were utilized as input for the linear discriminant analysis (LDA) classifier[23] to distinguish between ADs and HCs. Additionally, the E_{DD} features obtained from each regional mean time series for rs-fMRI data were fed into the LDA classifier to distinguish between participants at double-risk and those with no-risk. To evaluate the performance of the classifier, we employed a leave-one-subject-out (LOSO) scheme using accuracy as a metric. Under this scheme, one subject out of the S subjects was sequentially designated as the test set, while the remaining $S-1$ subjects served as training sets. During each LOSO loop, a two-sample t-test was conducted on the training set to identify discriminative features that could boost classification performance.[24]

Furthermore, the nonparametric permutation test was employed to determine the statistical significance of the obtained accuracies. Specifically, the class labels were permuted 1000 times across all subjects without replacement, and the entire classification procedure was repeated for each permutation. The final P values for accuracy metric were determined by calculating the frequency ratio of permutation accuracies that exceeded the true accuracy in all 1000 iterations. A statistical significant threshold of $P < 0.05$ was applied.

3. Results

3.1. BPVG analysis on simulation time series

3.1.1. BPVG analysis on periodic series

The sinusoidal signal, $y = \sin(5\pi x)$, was selected as a typical periodic time series. By setting the sampling interval to 0.01 and the sequence length to 1000, we obtained the sinusoidal series depicted in Fig. 2(a). After being transformed into BPVG, it was observed to manifest as a regular network, as shown in Fig. 2(b). The wave crest and trough of the sinusoidal signal exhibited the equal degree, thereby reflecting the symmetry of the time series to a certain extent. Furthermore, the degree distribution exhibited discreteness in Fig. 2(c) and can be quantified as 1.93 using E_{DD} (see Table 1). Hence, for a periodic sequence, the transformed BPVG can effectively preserve this characteristic and be visualized as a regular network.

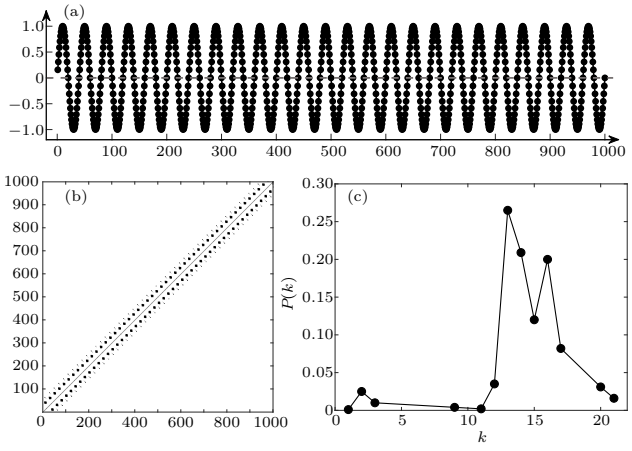


Fig. 2. (a) The black dotted line represents the sinusoidal signal $y = \sin(5\pi x)$ sampled at an interval of 0.01 with a sequence length of 1000, while the gray dashed line denotes the referenced baseline. (b) The adjacency matrix of the BPVG algorithm for the sinusoidal signal. (c) The degree distribution of BPVG algorithm constructed from the sinusoidal signal.

Table 1. The E_{DD} of BPVGs constructed from the used simulated time series.

Periodic series[a]	Random series[b]	Fractal series[c]			
		$H = 0.1$	$H = 0.4$	$H = 0.7$	$H = 0.9$
1.9314	2.7592	2.8472	3.2356	4.3015	5.6610

[a]The E_{DD} of periodic series is calculated on the sinusoidal signal, $y = \sin(5\pi x)$, with the sampling interval of 0.01 and the sequence length of 1000.
[b]The E_{DD} of random series is calculated on a randomly generated series conforming the standard normal distribution $N(0,1)$ with the sequence length of 1000.
[c]The E_{DD} of fractal series is calculated on the fractional Brownian motion signals at various fractal scales with the Hurst exponent of 0.1, 0.4, 0.7, and 0.9, and the sequence length of 5000.

3.1.2. BPVG analysis on random series

We generated a random series following the standard normal distribution $N(0,1)$ with a length of 1000 data points, as displayed in Fig. 3(a). The transformed BPVG exhibited a notable concentration of connections near the diagonal, accompanied by a random distribution, as depicted in Fig. 3(b). The degree distribution obtained from BPVG, as depicted in Fig. 3(c), exhibited a Poisson distribution at the front and an exponential distribution at the tail, with a summarized E_{DD} of 2.76. The random series can thus be transformed into a random network using the BPVG algorithm, enabling the capture and preservation of temporal randomness.

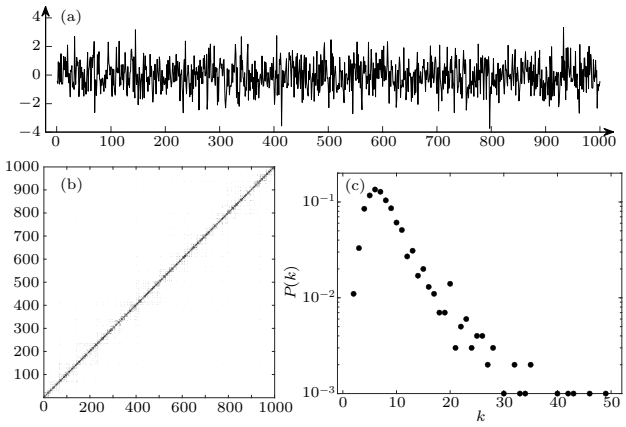


Fig. 3. (a) The random series conforms to the standard normal distribution with a sequence length of 1000. (b) The adjacency matrix of the BPVG algorithm for this random series. (c) The degree distribution of BPVG algorithm constructed from the random series.

3.1.3. BPVG analysis on fractal series

The fractional Brownian motion signals were generated with multiple fractal scales (*i.e.*, $H = 0.1$, 0.4, 0.7, and 0.9 in Fig. 4(a)), while ensuring a time series length of 5000. As illustrated in Fig. 4(b), the generated fractal Brownian series exhibited distinct power law characteristics in their network degree distributions after undergoing the BPVG transformation. Moreover, it was observed from Table 1 that the values of E_{DD} exhibited an increase as the Hurst index increased. This observation highlights the effectiveness of the BPVG algorithm in accurately capturing scale-free properties within fractal sequences and distinguishing sequences with different Hurst indices.

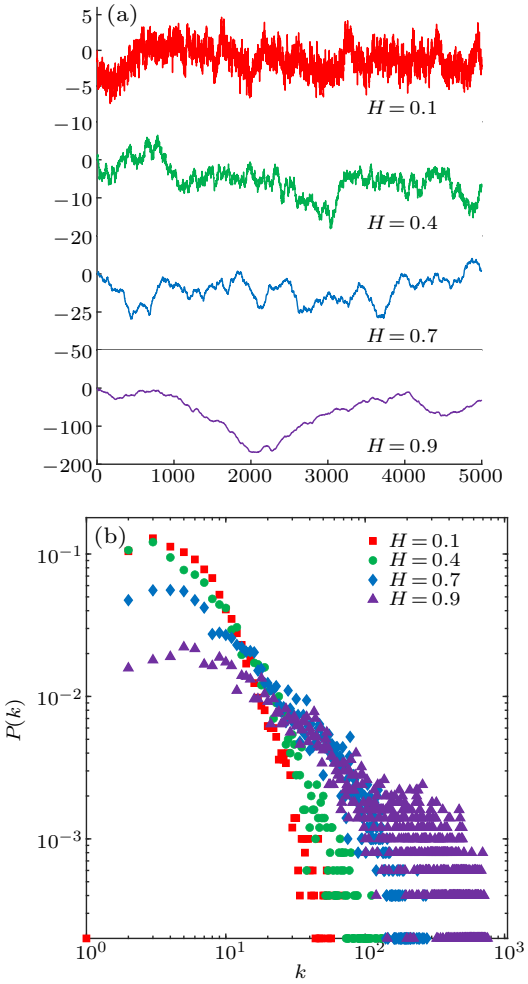


Fig. 4. (a) Illustrations of fractional Brownian motion signals at various fractal scales for $H = 0.1$, 0.4, 0.7, and 0.9, with a time series length of 5000. (b) Degree distribution of the BPVG algorithm constructed from these fractal Brownian time series.

3.2. BPVG analysis on real EEG time serie

In this study, a total of 150 features were extracted from each subject's EEG data for each channel, encompassing 30 segments across 5 frequency bands. Subsequently, these feature vectors of single-channel EEG data were individually fed into an LDA classifier using the LOSO scheme. The resulting classification accuracies are presented in Fig. 5. Notably, statistical significance was observed for 10 out of the total 19 channels (indicated by asterisks on corresponding amber bars in Fig. 5(a)). These significant channels are distributed across various brain regions, including Fp1, Fz, F4, T5, T6, P3, Pz, P4, O1, and O2, as depicted in Fig. 5(b). It is noteworthy that the classification accuracies achieved by F4 and O1 reached 78.46% and 81.54%, respectively, surpassing the highest benchmark accuracy of 77.01% provided in Ref. [16].

3.3. BPVG analysis on real rs-fMRI time series

After applying BPVG analysis to the rs-fMRI time series of each participant, we constructed a feature vector by integrating the E_{DD} features derived from the transformed BPVG

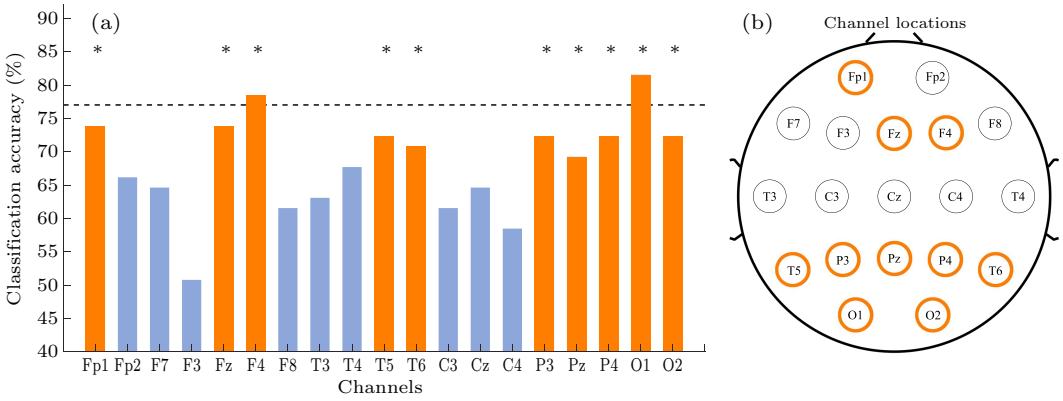


Fig. 5. Classification accuracy results of BPVG analysis for AD and HC using EEG time series. (a) Classification accuracy bar chart. The horizontal axis denotes the 19 EEG channel names, while the vertical axis indicates the percentage accuracy for each channel. Bars colored in amber signify statistical significance ($P < 0.05$) after conducting a permutation test, denoted by asterisks. The black dashed line represents the benchmark accuracy provided by the EEG dataset collection team. (b) Spatial distribution of EEG channels. Channels with significant accuracy are highlighted with thick amber circles and labeled boldly.

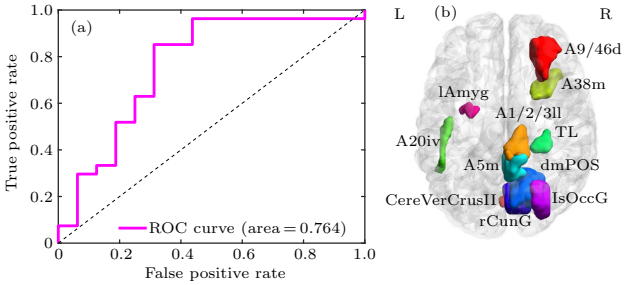


Fig. 6. Classification outcomes of BPVG analysis for adults categorized as double-risk and no-risk using rs-fMRI time series. Panel (a) illustrates the mean area under the receiver operating characteristic curve obtained from the analysis, while panel (b) delineates the 11 discriminative brain regions identified. IAmyg = lateral amygdala; A20iv = intermediate ventral area 20 of the inferior temporal gyrus; A9/46d = dorsal area 9/46 of the middle frontal gyrus; A38m = medial area 38 of the superior temporal gyrus; A1/2/3ll = lower limb areas 1/2/3 of the paracentral lobule; TL = lateral area of the posterior parahippocampal gyrus; A5m = medial area 5 of the precuneus; dmPOS = dorsomedial parietooccipital sulcus of the precuneus; CereVerCrusII = crus II vermis region in the cerebellum; rCunG = rostral cuneus gyrus in the medioventral occipital cortex; IsOccG = lateral superior occipital gyrus in the lateral occipital cortex; L = the left hemisphere; R = the right hemisphere.

matrices. Subsequently, these vectors were input into an LDA classifier using an LOSO scheme. As depicted in Fig. 6(a), our classifier achieved an average area under the ROC curve value of 0.764, with a classification accuracy of 76.74%. This performance was statistically significant ($P = 0.025$), as confirmed by permutation tests. Additionally, as illustrated in Fig. 6(b), the classifier identified discriminative ROIs across key brain regions, including the right frontal and parietal cortices, specifically highlighting the dorsal middle frontal gyrus (A9/46d.R), lower limb areas of the right paracentral lobule (A1/2/3ll.R), as well as specific regions within the precuneus such as its right medial area 5 (A5m.R) and dorsomedial parietooccipital sulcus (dmPOS.R). In addition, discriminative ROIs were observed in the temporal lobe structures including medial area of the superior temporal gyrus (A38m.R), intermediate ventral area of the left inferior temporal gyrus (A20iv.L), and lateral area of the posterior parahippocampal gyrus (TL.R). Notably, significant discriminative power was also found in the occipital lobe, such as the right rostral cuneus gyrus (rCunG.R) and the lateral superior occipital gyrus (IsOccG.R). Besides, discriminative activity was also observed in the left lateral amygdala (IAmyg.L), and the crus II vermis region within cerebellum (CereVerCrusII).

4. Discussion

The present study proposed a novel method called BPVG, which can effectively capture comprehensive information from time series for both above and below the baseline during their transformation into visibility graphs. We applied the BPVG analysis to three typical types of time series: periodic, random, and fractal. The results demonstrated that BPVG can successfully map periodic series into regular networks, random series into random networks, and fractal series into scale-free networks. Additionally, we also applied the BPVG method to analyze real EEG and rs-fMRI data and made intriguing discoveries. Regarding EEG data, more than 50% of single-channel EEG recordings exhibited statistically significant accuracy in distinguishing individuals with AD from HC. Remarkably, the classification accuracy achieved by channels F4 and O1 surpassed the benchmark accuracy provided by the data collection team. When applying BPVG to real rs-fMRI data, it demonstrated a statistically significant classification accuracy over 76% in distinguishing between participants at double-risk and those with no-risk. These findings validated the effectiveness of the proposed BPVG method.

The BPVG algorithm introduces a significant advancement by accurately capturing non-negligible information from time points below the baseline in the time series. It is worth noting that real physiological signals often exhibit signals below the baseline, and previous research has highlighted the physiological significance of these sub-baseline signals.[8,10] However, the NVG algorithm lacks the capability to effectively capture this aspect of the signal. In contrast, the BPVG algorithm addresses this limitation by analyzing both above

and below baseline time points in the time series. This comprehensive approach enables the construction of a network that captures a more extensive range of connectivity information across all time points. The superiority of the BPVG algorithm over the NVG algorithm is illustrated in Fig. 1, where it successfully incorporates connections between above and below baseline time points (*e.g.*, A–F) and between sub-baseline time points (*e.g.*, C–F), while eliminating spurious connections (*e.g.*, A–C). By considering both above and below baseline time points, the BPVG algorithm can effectively capture the connectivity patterns in the time series and preserve the inherent data structure information.

The results obtained from both simulation and real EEG and rs-fMRI time series support the effectiveness of the BPVG method. On the one hand, the BPVG method demonstrates its capability to discriminate between periodic, random, and fractal sequences by capturing distinct degree distribution curves in the transformed network (Figs. 2–4), which is crucial for understanding the underlying dynamics of the time series. Moreover, the differences among these sequence types can be quantified using the E_{DD} feature (Table 1). The E_{DD} feature measures the diversity of connections within a BPVG network,[25] with higher entropy indicating a more diverse system. Notably, periodic series exhibit the minimum E_{DD} value while fractal series display maximum E_{DD} values, consistent with existing knowledge.

On the other hand, upon applying BPVG to real EEG channel series, we observed a predominant localization of channels with significant classification accuracies in specific brain regions. These regions covered part of the anterior frontal region (*i.e.*, Fp1), part of the frontal region (*i.e.*, F4 and Fz), part of the temporal region (*i.e.*, T5 and T6), the parietal region (*i.e.*, P3, P4, and Pz), and the occipital region (*i.e.*, O1 and O2) , all of which have been reported to play significant roles in AD detection.[26–29] Previous studies have provided evidence supporting the importance of these regions in distinguishing AD patients from HCs. Abásolo *et al.*[26] found that EEG signals from P3, P4, O1, and T5 channels in AD patients exhibited significantly lower Lempel-Ziv complexity compared to HC. Jeong *et al.*[27] reported reduced local information transmission in the frontal and antero-temporal regions, particularly in the right hemisphere and between interhemispheric regions, along with lower EEG complexity in AD patients. Furthermore, Choi *et al.*[28] demonstrated a moderate correlation between mini-mental state examination scores of AD patients and median frequency, peak frequency, and alpha-to-theta ratio measured at the Fp1 region using resting-state EEG. Ando *et al.*[29] combined multiscale entropy and multifractal analyses to show a significantly higher smoothness index in the AD group at F3, Fz, F4, C3, C4, P3, Pz, and P4 channels. The findings of our study are consistent with previous research, underscoring the high sensitivity of BPVG in capturing the intricate dynamics of EEG signals. Notably, our results indicate that using a single-channel EEG recording at either the F4 or O1 channel can achieve better classification accuracies than the highest benchmark accuracy. This finding suggests that even single-channel EEG data might be sufficient for recognizing AD,[30,31] potentially simplifying the diagnostic process and increasing its accessibility.

In our analysis of real rs-fMRI time series, we have identified several functionally relevant brain regions that exhibit significant discriminative power. Notably, the frontal cortex, specifically the A9/46d.R region, plays a crucial role in executive functions and has been observed to atrophy in AD patients.[32,33] This atrophy is likely driven by APOE–PICALM genotype interactions,[34] which are known to exacerbate amyloid-beta ($A\beta$) deposition and synaptic dysfunction in prefrontal regions during early AD pathogenesis.[35] The BPVG- detected network alterations in A9/46d.R may thus reflect early $A\beta$-driven neurodegeneration, providing a novel link between genetic risk and network topology. Clarke *et al.*[36] emphasized the right paracentral lobule as a critical hub in individuals with both the APOE-ε4 genotype and a family history of dementia. Our findings align with this observation and extend it by associating hub disruption with metabolic risk factors, which may synergistically accelerate $A\beta$ pathology in this region. The precuneus region, including the A5m.R and dmPOS.R areas, is essential for episodic memory and self-referential processing.[37] Its disrupted BPVG connectivity in the double-risk group may correspond to tau pathology and default mode network (DMN) disintegration, as tau accumulation preferentially targets DMN hubs in preclinical AD.[38] This aligns with studies showing that APOE-ε4 carriers exhibit reduced DMN functional connectivity even before cognitive decline,[39] suggesting that BPVG captures early network vulnerability to AD-specific proteinopathy. Additionally, temporal lobe structures, such as the A38m.R and A20iv.L, are crucial for auditory processing and semantic memory,[40] with TL.R sensitivity to AD-related changes potentially reflecting entorhinal cortex tau spread.[41] Similarly, the occipital regions (*i.e.*, rCunG.R and IsOccG.R), though primarily contribute to visual processing, show AD-related atrophy linked to posterior cortical $A\beta$ deposition.[42,43] Finally, the IAmyg.L and CereVerCrusII abnormalities may indicate comorbid emotional dysregulation and motor coordination deficits in high-risk individuals, as limbic-cerebellar circuits are increasingly recognized in AD progression.[44,45] These findings not only highlight region-specific AD pathology but also demonstrate the ability of BPVG to map multiscale network disruptions ($A\beta$/tau spread, genetic-metabolic interactions) underlying dementia risk.

The superior performance of the BPVG method could be

attributed to two potential reasons. Firstly, the unique capability of the BPVG to incorporate both above and below baseline data points in its analysis is crucial for obtaining a comprehensive view of the time series. This inclusive strategy ensures that the original data's structural integrity remains intact during the conversion to a visibility graph, thereby preventing the introduction of spurious connections or the omission of valid ones. Consequently, the resulting networks are more representative and accurately reflect both linear and nonlinear temporal dynamics inherent in the time series. This heightened fidelity in network construction significantly enhances our understanding of the physiological mechanisms and provides a clearer depiction of intricate interconnections within the data. Secondly, the conversion of BPVG facilitates the application of robust network analytical techniques that excel at uncovering intricacies in time series analysis. The method's dual-scale analytical capabilities, encompassing both micro and macro fluctuations, enable a comprehensive characterization that distinguishes it from other approaches which may overlook subtle aspects of signal structure. In our investigation, we employed E_{DD} as a comprehensive metric to quantify degree distribution heterogeneity and complexity within the network, providing an assessment tool for discerning minute alterations in brain activity often pivotal in neurological disorders. By integrating BPVG conversion with advanced network analysis, our study has not only enhanced diagnostic potential of EEG data but also shed light on multifaceted nature underlying neurological conditions such as AD.

Despite the promising results demonstrated by the BPVG method in this study, several limitations should be acknowledged. Firstly, the current implementation of the BPVG results in an unweighted network. Incorporating additional information, such as slope or view angle, into the network construction framework[46] could potentially yield more discriminative features. Secondly, this study only applied BPVG to single-channel EEG data and separate rs-fMRI time series, while future research should consider integrating BPVG with multilayer network analysis to capture interconnections between different channels or ROIs.[47,48] Thirdly, while this study extracted the E_{DD} feature, numerous other significant network features[49] warrant exploration to broaden the application scope of BPVGs. Furthermore, future investigations should consider expanding the sample size, exploring additional neurological disorders beyond AD, and integrating BPVG with other graph-theoretical and machine learning approaches to enhance its diagnostic capabilities.[50] Notably, emerging neuromorphic architectures offer innovative implementation pathways. Recent research on double stochastic nanowire networks[51] has illustrated how physical network reconfiguration can enhance temporal processing via dynamic conductance modulation. This indicates potential synergies between such approaches and BPVG's visibility-based topology, enabling the development of hybrid systems that integrate geometric pattern analysis with physically dynamic computing for multi-modal neural signal processing.

5. Conclusions

In summary, we propose a novel method named as the BPVG to analyze temporal patterns in the time series of the brain activity, including EEG and rs-fMRI. The BPVG method effectively captures comprehensive structural information from both above and below the baseline, while preserving this information during its transformation into a visibility graph. We have validated its ability to capture information from both sides of the baseline across simulated periodic, random, and fractal time series. Furthermore, by applying the BPVG to real EEG and rs-fMRI time series for early detection of AD and non-demented adults with varying dementia risk, we demonstrate its practical value. In conclusion, the proposed BPVG method could serve as a valuable tool for analyzing time series and enhancing our understanding of the neurological foundations underlying physiological signals.

Acknowledgements

Project supported by the National Key Research and Development Program of China (Grant No. 2023YFF1204803), the Natural Science Foundation of Jiangsu Province, China (Grant No. BK20190736), the Fundamental Research Funds for the Central Universities (Grant No. NJ2024029), and the National Natural Science Foundation of China (Grant Nos. 81701346 and 62201265).

Data were provided by PEARL-Neuro Database from Nencki Institute of Experimental Biology PAS, Poland.

References

[1] Lacasa L, Luque J, Luque B, Ballesteros F and Nu O J C 2008 *Proc. Natl. Acad. Sci. USA* **105** 4972
[2] Li X and Dong Z 2011 *Phys. Rev. E* **84** 062901
[3] Shao Z G 2010 *Appl. Phys. Lett.* **96** 073703
[4] Ahmadlou M, Adeli H and Adeli A 2010 *Journal of Neural Transmission* **117** 1099
[5] Zhu G, Li Y and Wen P Paul 2014 *Computer Methods and Programs in Biomedicine* **115** 64
[6] Sannino S, Stramaglia S, Lacasa L and Marinazzo D 2017 *Network Neuroscience* **1** 208
[7] Zheng M, Domanskyi S, Piermarocchi C and Mias G I 2021 *Sci. Rep.* **11** 5623
[8] Schridde U, Khubchandani M, Motelow J E, Sanganahalli B G, Hyder F and Blumenfeld H 2008 *Cerebral Cortex* **18** 1814
[9] Rathakrishnan R, Moeller F, Levan P, Dubeau F and Gotman J 2010 *Epilepsia* **51** 1837
[10] Gründler T O J, Cavanagh J F, Figueroa C M, Frank M J and Allen J J B 2009 *Neuropsychologia* **47** 1978
[11] Falkenstein M, Hoormann J, Christ S and Hohnsbein J 2000 *Biological Psychology* **51** 87
[12] Hasson U, Iacovacci J, Davis B, Flanagan R, Tagliazucchi E, Laufs H and Lacasa L 2018 *Sci. Rep.* **8** 3557
[13] Zhou T, Jin N, Gao Z and Luo Y 2012 *Acta Sin. Phys.* **61** 030506 (in Chinese)

[14] Andreas M, D. T K, Nikolaos G, G. T M, Theodora A, Panagiotis I and T. T A 2021 *Diagnostics* **11** 1437

[15] Tzimourta K D, Afrantou T, Ioannidis P, Karatzikou M, Tzallas A T, Giannakeas N, Astrakas L G, Angelidis P, Glavas E, Grigoriadis N, Tsalikakis D G and Tsipouras M G 2019 *Computers and Electrical Engineering* **76** 198

[16] Miltiadous A, Tzimourta K D, Afrantou T, Ioannidis P, Grigoriadis N, Tsalikakis D G, Angelidis P, Tsipouras M G, Glavas E, Giannakeas N and Tzallas A T 2023 *Data* **8** 95

[17] Miltiadous A, Tzimourta K D, Afrantou T, Ioannidis P, Grigoriadis N, Tsalikakis D G, Angelidis P, Tsipouras M G, Glavas E, Giannakeas N and Tzallas A T 2023 *OpenNeuro*

[18] Dzianok P and Kublik E 2024 *Scientific Data* **11** 276

[19] Yan C G, Wang X D, Zuo X N and Zang Y F 2016 *Neuroinformatics* **14** 339

[20] Yan C and Zang Y 2010 *Frontiers in Systems Neuroscience* **4** 13

[21] Ashburner J 2007 *NeuroImage* **38** 95

[22] Fan L, Li H, Zhuo J, Zhang Y, Wang J, Chen L, Yang Z, Chu C, Xie S, Laird A R, Fox P T, Eickhoff S B, Yu C and Jiang T 2016 *Cerebral Cortex* **26** 3508

[23] Lin W, Gao Q, Du M, Chen W and Tong T 2021 *Computers in Biology and Medicine* **134** 104478

[24] Dai Z, Yan C, Wang Z, Wang J, Xia M, Li K and He Y 2012 *NeuroImage* **59** 2187

[25] Jones C and Wiesner K 2022 *Entropy* **24** 1182

[26] Abásolo D, Hornero R, Gómez C, García M and López M 2006 *Medical Engineering & Physics* **28** 315

[27] Jeong J, Gore J C and Peterson B S 2001 *Clinical Neurophysiology* **112** 827

[28] Choi J, Ku B, You Y G, Jo M, Kwon M, Choi Y, Jung S, Ryu S, Park E, Go H, Kim G, Cha W and Kim J U 2019 *Sci. Rep.* **9** 10468

[29] Ando M, Nobukawa S, Kikuchi M and Takahashi T 2021 *Frontiers in Neuroscience* **15** 667614

[30] Del Percio C, Lopez S, Noce G, Lizio R, Tucci F, Soricelli A, Ferri R, Nobili F, Arnaldi D, Famà F, Buttinelli C, Giubilei F, Marizzoni M, Güntekin B, Yener G, Stocchi F, Vacca L, Frisoni G B and Babiloni C 2023 *Clinical EEG and Neuroscience* **54** 21

[31] Kim H T, Kim B Y, Park E, Kim J W, Hwang E W, Han S and Cho S 2005 *Future generation computer systems* **21** 1124

[32] Wong S, Bertoux M, Savage G, Hodges J R, Piguet O and Hornberger M 2016 *Journal of Alzheimer's Disease* **51** 889

[33] Wu H, Song Y, Chen S, Ge H, Yan Z, Qi W, Yuan Q, Liang X, Lin X and Chen J 2022 *Frontiers in Neuroscience* **16** 876568

[34] Morgen K, Ramirez A, Frölich L, Tost H, Plichta M M, Kölsch H, Rakebrandt F, Rienhoff O, Jessen F, Peters O, Jahn H, Luckhaus C, Hüll M, Gertz H J, Schröder J, Hampel H, Teipel S J, Pantel J, Heuser I, Wiltfang J, Rüther E, Kornhuber J, Maier W and Meyer-Lindenberg A 2014 *Alzheimer's & Dementia* **10** S269

[35] Liu Y B, Wang X J, Tan L, Tan C C and Xu W 2023 *Journal of Alzheimer's Disease* **96** 1651

[36] Clarke H, Messaritaki E, Dimitriadis S I and Metzler-Baddeley C 2022 *Brain Connectivity* **12** 26

[37] Cavanna A E and Trimble M R 2006 *Brain* **129** 564

[38] Yu M, Sporns O and Saykin A J 2021 *Nat. Rev. Neurol.* **17** 545

[39] Chiesa P A, Cavedo E, Vergallo A, Lista S, Potier M C, Habert M O, Dubois B, Thiebaut de Schotten M and Hampel H 2019 *Alzheimer's & Dementia* **15** 940

[40] Chan D, Fox N C, Scahill R I, Crum W R, Whitwell J L, Leschziner G, Rossor A M, Stevens J M, Cipolotti L and Rossor M N 2001 *Annals of Neurology* **49** 433

[41] Fung C W, Guo J, Fu H, Figueroa H Y, Konofagou E E and Duff K E 2020 *Sci. Adv.* **6** eabc8098

[42] Uhlhaas P J, Pantel J, Lanfermann H, Prvulovic D, Haenschel C, Maurer K and Linden D E J 2008 *Dementia and Geriatric Cognitive Disorders* **25** 465

[43] Jeong S H, Cha J, Jung J H, Yun M, Sohn Y H, Chung S J and Lee P H 2023 *JAD* **94** 1133

[44] Toniolo S, Serra L, Olivito G, Marra C, Bozzali M and Cercignani M 2018 *Frontiers in Cellular Neuroscience* **12** 430

[45] Tang F, Zhu D, Ma W, Yao Q, Li Q and Shi J 2021 *Frontiers in Neurology* **12** 645171

[46] Bose R, Samanta K, Modak S and Chatterjee S 2021 *IEEE Journal of Biomedical and Health Informatics* **25** 685

[47] Gao Z K, Guo W, Cai Q, Ma C, Zhang Y B and Kurths J 2019 *Chaos* **29** 073119

[48] Song Z, Deng B, Wang J and Wang R 2019 *IEEE Transactions on Biomedical Engineering* **66** 41

[49] Wen T, Chen H and Cheong K H 2022 *Nonlinear Dyn.* **110** 2979

[50] Xuan Q, Zhou J, Qiu K, Chen Z, Xu D, Zheng S and Yang X 2022 *IEEE Transactions on Network Science and Engineering* **9** 1516

[51] Tang J F, Xia L, Li G L, Fu J, Duan S and Wang L 2024 *Chin. Phys. B* **33** 037302